

Paper

Theoretical Analysis of Thermal Conductivity of Graphite-containing Refractory Brick

**Yoshihiro HIRATA, Naoki MATSUNAGA, Jyoki YOSHITOMI and
Tsuneo KAYAMA**

Journal of the Technical Association of Refractories, Japan

Vol. 31 No. 3

p. 156 - 163

Theoretical Analysis of Thermal Conductivity of Graphite-containing Refractory Brick

Yoshihiro HIRATA, Naoki MATSUNAGA, Jyoki YOSHITOMI* and Tsuneo KAYAMA*

Abstract

Thermal conductivities were calculated for the refractory brick of carbon-alumina-pore system, carbon-alumina-silicon carbide-pore system and carbon-alumina-silica-pore system. The proposed conduction model was extended from our previous two phase conduction model developed for solid material with particulate inclusion. The three or four phase model reflects the microstructure of the refractory brick and predicts the maximum and minimum conductivities in parallel and perpendicular directions to c-axis of graphite. The calculated values were plotted in the triangle of thermal conductivities of graphite-alumina-pores systems as functions of alumina content and porosity. The thermal conductivity of refractory brick along perpendicular direction to c-axis of graphite decreases at higher fractions of alumina grains and pores. This calculated result is explained by the decrease of volume fraction of graphite with a higher thermal conductivity. The experimental thermal conductivities were measured in the range predicted from the calculation and very close to the average value of calculated maximum and minimum conductivities.

Key words: Thermal conductivity, Refractory brick, Carbon, Pore, Alumina, Silicon carbide, Silica

1. Introduction

Thermal conductivity is an important property of material, which is used to design a structure of assembly of functional parts or to estimate a temperature gradient in the material at a given energy flux. Wang and Pan¹⁾ summarize mixing rules of thermal conductivity for composite materials. In their review, parallel model, series model, EMT model (effective medium theory), Maxwell model, Hamilton model and reciprocity model are discussed. Wang et al.²⁾ proposed a structural model of effective thermal conductivity for heterogeneous materials with two continuous phases. This model provides the effective thermal conductivity of three phase systems (phases 1, 2: continuous phase, 3: dispersed phase). Bouchair³⁾ also proposed a model of thermal conductivity of fired clay hollow bricks for enhanced thermal insulation. He calculated the thermal resistance of conductive wall based on the electrical resistance analogy. On the other hand, Hirata derived a theoretical effective thermal conductivity of material with particle inclusion in a continuous phase⁴⁾. The derived thermal conductivity of two phase system (κ_{ap} ($\text{W}\cdot\text{m}^{-1}\cdot\text{K}^{-1}$), Eq. (1)) can be expressed by three parameters of κ_1 ($\text{W}\cdot\text{m}^{-1}\cdot\text{K}^{-1}$) for inclusion, κ_2 ($\text{W}\cdot\text{m}^{-1}\cdot\text{K}^{-1}$) for a continuous phase and volume fraction v_1 (vol%) of inclusion,

$$\kappa_{ap} = \kappa_2 - \kappa_2 v_1^{2/3} \left[1 - \frac{1}{1 - v_1^{1/3} \left(1 - \frac{\kappa_2}{\kappa_1} \right)} \right] \quad (1)$$

Equation (1) provides a good agreement with the measured κ_{ap} for AlN particle-dispersed SiO₂ system. On the other hand, refractory brick consists of three or four phase systems such as carbon-Al₂O₃-pore, carbon-Al₂O₃-SiC-pore or carbon-Al₂O₃-SiO₂-pore, where pore is treated as one phase. The purpose of

this paper is to propose an effective thermal conduction model of refractory brick as functions of thermal conductivities and volume fractions of included phases, which reveals the effects of included phases on the thermal conductivity of refractory brick. The theoretical model assists the designing of microstructures and phase compositions of multi phase refractory brick. In this paper, an effective thermal conduction model for refractory brick of three phase systems or four phase systems is derived from Eq. (1) for two phase systems. The calculated conductivity is compared with the experimentally measured conductivity.

2. Composition, thermal conductivity and microstructure of refractory brick

Table 1 shows the compositions and thermal conductivities of three kinds of refractory brick fabricated by Krosaki Harima Corporation. Samples A, B and C consisted of carbon-Al₂O₃-pore, carbon-Al₂O₃-SiC-pore and carbon-Al₂O₃-SiO₂-pore systems, respectively. The volume fraction of each phase was determined from its chemical composition (mass%) and true density. The thermal conductivities measured at room temperature were in the range from 27 to 45 $\text{W}\cdot\text{m}^{-1}\cdot\text{K}^{-1}$. As seen in Table 1, the two measured conductivities for each sample were slightly different, and this is related to the preferred orientation of graphite structure during the processing of refractory brick. The thermal conductivities were measured by laser flash method for sample A (Netzsch Co., Selb, Germany, LFA 457 MicroFlash) and hot disk method for samples B and C (Kyoto Electronics Manufacturing Co., Ltd., Kyoto, Japan, TPS2500S) at Krosaki Harima Corporation. The thermal conductivity of each phase is also shown in Table 1. Silicon carbide has the highest value and air (pore) has the lowest value

Department of Chemistry, Biotechnology, and Chemical Engineering, Kagoshima University, 1-21-40 Korimoto, Kagoshima 890-0065, Japan

*Krosaki Harima Corporation,

156 1-1 Yahatanishi-ku, Higashihama, Kitakyushu, Fukuoka 806-8586, Japan

Received Apr. 26, 2011

Accepted Oct. 21, 2011

Table 1 Composition and thermal conductivity of refractory brick

Phase	Composition / vol%			Thermal conductivity / $W \cdot m^{-1} \cdot K^{-1}$	
		sample A	sample B	sample C	
Graphite	v_2 (carbon matrix)	29.5	32.5	35.6	κ_2 (carbon matrix) 129 ^{a)} , 98 ^{b),5)}
Amorphous carbon		7.4	7.5	7.4	
Alpha- Al_2O_3	v_1	43.2	36.5	22.8	κ_1 36 ⁵⁾
Pores (closed and open pores)	v_3	20.0	19.9	15.1	0.0265 (air) ⁵⁾
SiC	v_4	0	3.6	0	κ_4 168 ⁶⁾
SiO ₂ (quartz glass)	v_5	0	0	19.1	κ_5 1.38 ⁶⁾
Thermal conductivity of sample/ $W \cdot m^{-1} \cdot K^{-1}$ d)		{ 32.3 28.2	{ 38.8 27.4	{ 44.7 34.5	

a), b): along perpendicular ($129 W \cdot m^{-1} \cdot K^{-1}$) and parallel ($98 W \cdot m^{-1} \cdot K^{-1}$) directions to c-axis of graphite
c), d): measured by Krosaki Harima Corporation

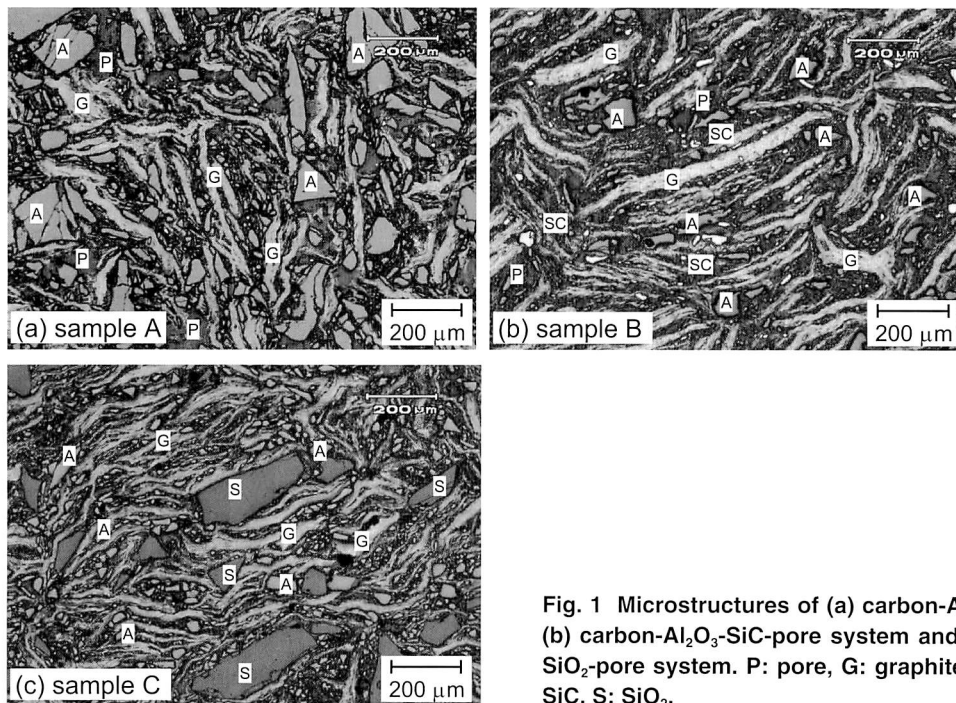


Fig. 1 Microstructures of (a) carbon- Al_2O_3 -pore system, (b) carbon- Al_2O_3 -SiC-pore system and (c) carbon- Al_2O_3 -SiO₂-pore system. P: pore, G: graphite, A: alumina, SC: SiC, S: SiO₂.

of thermal conductivity. In this paper, a same thermal conductivity of air is given for closed and open pores. Graphite has the different two types of thermal conductivities along the perpendicular and parallel directions to c-axis of graphite. As compared with graphite, amorphous carbon which was produced from the organic resin added as a binder, has a significantly low thermal conductivity.

Figure 1 shows the microstructures of refractory brick. Graphite has a lamella structure, reflecting the characteristics of graphite structure. The elongated direction is perpendicular to c-axis of graphite. Pores (30–50 μm size), Al_2O_3 grains (50–70 μm size) and SiC grains (15–60 μm size) were well dispersed in the carbon matrix. SiO₂ grains were larger (60–350 μm) in the size than Al_2O_3 or SiC grains and also dispersed in the carbon matrix.

3. Thermal conduction model of three phase systems

3.1 Basic structural model

Figure 2(a) shows a simple cubic inclusion model with a m length in one cubic box with length $1/p$ (m^3). The number p corresponds to the number of inclusion along one direction of cubic matrix. In three phase systems, pores are included in the continuous matrix (Fig. 2(c)). In this model structure, κ_1 in Eq. (1) is changed to κ_3 (thermal conductivity of air). That is, the thermal conductivity of a continuous matrix containing pores (κ_{ap}) is represented by Eq. (2),

$$\kappa_{ap} = \kappa_2 - \kappa_2 v_p^{2/3} \left[1 - \frac{1}{1 - v_p^{1/3} \left(1 - \frac{\kappa_2}{\kappa_3} \right)} \right] \quad (2)$$

where v_p is related to the volume fractions of matrix (v_2) and pores (v_3) by Eq. (3).

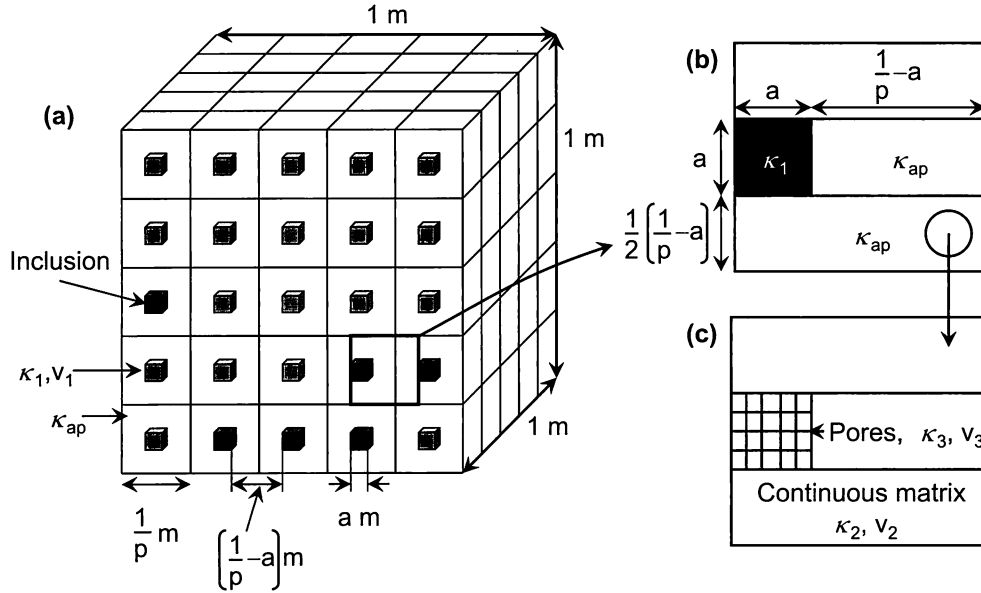


Fig. 2 (a) Model structure of material with three phases where (b) simple cubic inclusion with length a is dispersed in (c) a continuous matrix containing pores. a : length in one cubic box with length $1/p$, p : number of inclusion along one direction of cubic matrix, κ_1 : thermal conductivity of particle inclusion, κ_2 : thermal conductivity of a continuous phase, κ_3 : thermal conductivity of air, κ_{ap} : thermal conductivity of a continuous matrix containing pores (Eq. (2)), v_1 : volume fraction of particle inclusion, v_2 : volume fraction of carbon matrix (graphite plus amorphous carbon), v_3 : volume fraction of pore.

$$v_p = \frac{v_3}{v_2 + v_3} \quad (3)$$

The effective thermal conductivity of three phase system (κ_b) shown in Fig. 2(b) is also represented by Eq. (4).

$$\kappa_b = \kappa_{ap} - \kappa_{ap} v_1^{2/3} \left[1 - \frac{1}{1 - v_1^{1/3} \left(1 - \frac{\kappa_{ap}}{\kappa_1} \right)} \right] \quad (4)$$

where κ_1 is the thermal conductivity of particle inclusion and v_1 is the volume fraction of particle inclusion in three phase systems. The volume fractions of carbon matrix (v_2 , graphite plus amorphous carbon), pore (v_3) and Al_2O_3 (v_1) in three phase refractory brick are given in Table 1.

3.2 Influence of structure of graphite on thermal conductivity of carbon matrix

Figure 3 shows a model structure of carbon matrix consisting of graphite and amorphous carbon. Black arrows show the directions of flux of thermal energy. As seen in Fig. 1, graphite has a lamella structure which affects the thermal conductivity of carbon matrix. On the other hand, amorphous carbon provides an isotropic thermal conductivity. The thermal conductivity of carbon matrix along direction I in Fig. 3 is given by Eq. (5),

$$\kappa_c(\text{I}) = \frac{\kappa_g(\text{I})\kappa_{ac}}{\kappa_g(\text{I})l_2 + \kappa_{ac}l_1} \quad (5)$$

where $\kappa_g(\text{I})$ and κ_{ac} are the thermal conductivities of graphite along the parallel direction to c-axis ($98 \text{ W} \cdot \text{m}^{-1} \cdot \text{K}^{-1}$) and amorphous carbon, respectively. The parameters of l_1 and l_2 are expressed by Eqs. (6) and (7), respectively,

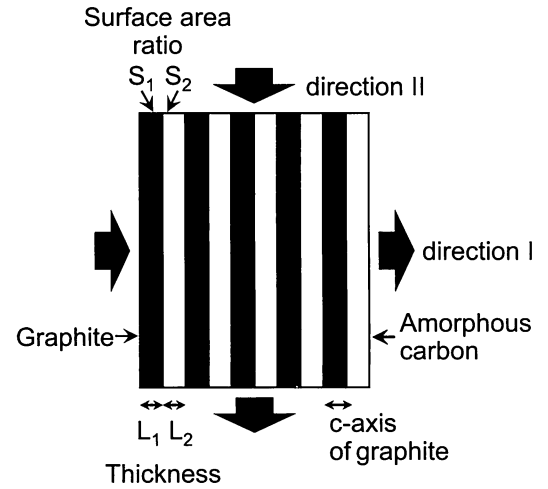


Fig. 3 Model structure of laminated matrix with graphite and amorphous carbon. L_1 : thickness of graphite layer, L_2 : thickness of amorphous carbon layer, S_1 : surface area ratio of graphite in direction II, S_2 : surface area ratio of amorphous carbon in direction II.

$$l_1 = \frac{L_1}{L_1 + L_2} \quad (6)$$

$$l_2 = \frac{L_2}{L_1 + L_2} \quad (7)$$

where L_1 and L_2 are the thickness of graphite and amorphous carbon layer, respectively. The l_1 and l_2 values are determined from their volume fractions.

On the other hand, the thermal conductivity of carbon matrix along direction II in Fig. 3 is given by Eq. (8),

$$\kappa_c(\text{II}) = \kappa_g(\text{II})S_1 + \kappa_{ac}S_2 = \kappa_{ac} + (\kappa_g(\text{II}) - \kappa_{ac})S_1 \quad (8)$$

where $\kappa_g(\text{II})$ is the thermal conductivity of graphite along the

perpendicular direction to c-axis ($124 \text{ W} \cdot \text{m}^{-1} \cdot \text{K}^{-1}$), and S_1 and S_2 are the ratio of surface area of graphite and amorphous carbon in direction II, respectively ($S_1 + S_2 = 1$). The κ_c (I) or κ_c (II) value is substituted for κ_2 in Eq. (2) to reflect the influence of structure of graphite.

3.3 Calculated thermal conductivity for three phase systems

Thermal conductivities of carbon- Al_2O_3 -pore system (sample A) were calculated using Eq. (4) for two directions I and II in Fig. 3. In sample A, the values of l_1 and l_2 were 0.7995 and 0.2005, respectively. S_1 and S_2 were also 0.7995 and 0.2005, respectively. As a result, κ_c (I) in Eq. (5) and κ_c (II) in Eq. (8) were calculated to be 17.9 and $104.0 \text{ W} \cdot \text{m}^{-1} \cdot \text{K}^{-1}$, respectively. These values were treated as κ_2 in Eq. (2). Furthermore, the determined κ_{ap} was used in Eq. (4) to calculate the effective thermal conductivity κ_b .

Figure 4 shows the calculated κ_b of sample A in directions I (a) and II (b) in a model structure (Fig. 3) as functions of Al_2O_3 content and pore volume. The indicated three points in Fig. 4 represent the thermal conductivities of (i) Al_2O_3 inclusion ($36 \text{ W} \cdot \text{m}^{-1} \cdot \text{K}^{-1}$), (ii) carbon matrix ($17.9 \text{ W} \cdot \text{m}^{-1} \cdot \text{K}^{-1}$ in (a), $104.0 \text{ W} \cdot \text{m}^{-1} \cdot \text{K}^{-1}$ in (b)) and (iii) pore ($0.0265 \text{ W} \cdot \text{m}^{-1} \cdot \text{K}^{-1}$), respectively. The line connecting the two points (i–ii, ii–iii and i–iii) shows κ_b of two phase systems: carbon- Al_2O_3 , carbon-pore and Al_2O_3 -pore. In the case of v_3 (pore volume) = 0 vol%, it is interpreted that the addition of Al_2O_3 grains enhances κ_b in direction I (Fig. 4(a), points ii–i) and reduces κ_b in direction II (Fig. 4(b), points ii–i). This tendency of κ_b depends on the difference of thermal conductivities between carbon matrix (κ_2) and Al_2O_3 inclusion (κ_1). Figure 4(a) and (b) correspond to the relation of $\kappa_2 < \kappa_1$, $\kappa_2 > \kappa_1$, respectively. The introduction of pores in dense carbon- Al_2O_3 system decreases κ_b in both the directions I and II at a similar Al_2O_3 content (v_1). The interesting

tendency in both the directions is that κ_b at a given v_3 decreases suddenly at a critical volume fraction of Al_2O_3 grains. The interpretation is clearly understood by the structural scheme shown in Fig. 5 and explained in a later sentence. The decrease of κ_b with increasing Al_2O_3 volume fraction is explained by the disappearance of carbon matrix from the refractory brick and the three phase system (carbon- Al_2O_3 -pore) changes into two phase system (Al_2O_3 -pore) at a critical v_1 value.

Figure 5(a)-(d) show the schematic structures of refractory brick (carbon- Al_2O_3 -pore system) along the κ_b line at $v_3 = 30$ vol% in direction I. At point (a) ($v_1 = 0$ vol%), pores of $v_3 =$

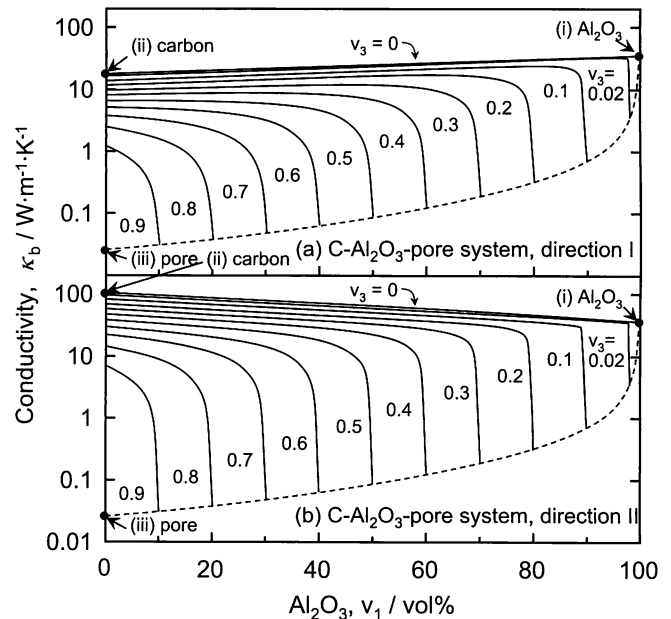


Fig. 4 Calculated conductivity of carbon- Al_2O_3 -pore system. v_1 : volume fraction of Al_2O_3 , v_3 : volume fraction of pore, κ_b : calculated thermal conductivity of carbon- Al_2O_3 -pore system.

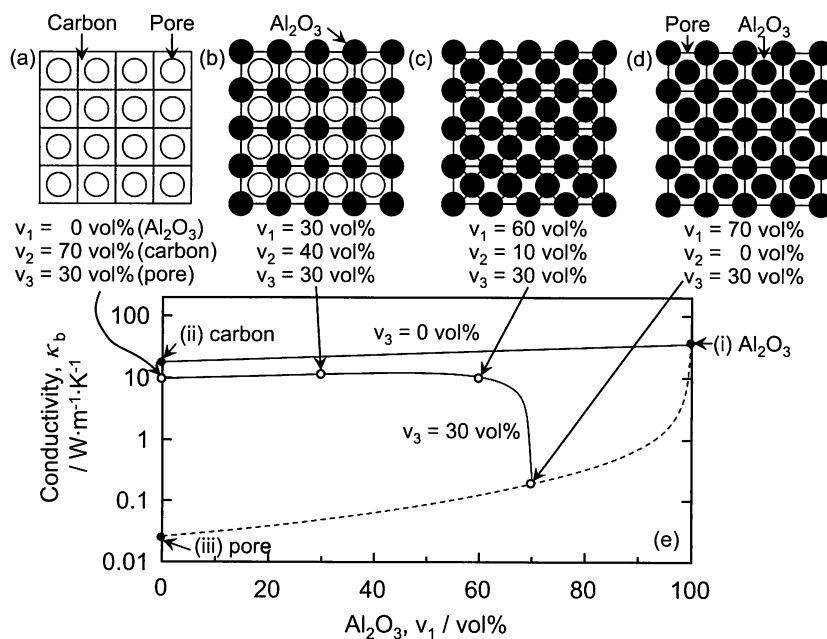


Fig. 5 Relationship between model structure and calculated conductivity for carbon- Al_2O_3 -pore system. v_1 : volume fraction of Al_2O_3 , v_2 : volume fraction of carbon matrix (graphite plus amorphous carbon), v_3 : volume fraction of pore, κ_b : calculated thermal conductivity of carbon- Al_2O_3 -pore system.

30 vol% are dispersed in a continuous carbon matrix. The addition of Al_2O_3 grains in carbon matrix, which causes the decrease of volume fraction of carbon matrix at a constant pore volume, increases slightly κ_b because of κ_{ap} (pore-containing carbon matrix) $< \kappa_1$ (Al_2O_3 grains). However, κ_b value starts to decrease above $v_1 = 60$ vol% (Fig. 5(c)) and reaches the lowest value at $v_1 = 70$ vol% where carbon matrix disappears (Fig. 5(d)). This tendency reflects the decrease of κ_{ap} in Eq. (2) from $9.89 \text{ W} \cdot \text{m}^{-1} \cdot \text{K}^{-1}$ at $v_1 = 0$ vol% to $0.0265 \text{ W} \cdot \text{m}^{-1} \cdot \text{K}^{-1}$ of air (κ_3) at $v_1 = 70$ vol%. In the v_1 range of 60 to 70 vol%, the matrix phase changes from carbon to air and Al_2O_3 grains with a higher thermal conductivity is separated from another Al_2O_3 grains by air. Therefore, introduction of uniformly distributed pores has a significant effect to decrease κ_b of dense two phase systems. This is seen clearly in the case of only $v_3 = 2$ vol% in Fig. 4(a) and (b).

4. Thermal conductivity of four phase systems

4.1 Theoretical model

In this section, we introduce κ_b for four phase systems. At first, the thermal conductivity (κ_m) of pore-containing carbon matrix phase is given by Eq. (9),

$$\kappa_m = \kappa_c - \kappa_c v_p^{2/3} \left[1 - \frac{1}{1 - v_p^{1/3} \left(1 - \frac{\kappa_c}{\kappa_p} \right)} \right] \quad (9)$$

where κ_c and κ_p are the thermal conductivities of carbon matrix (depending on the structural orientation of graphite, Eq. (5) or Eq. (8)) and pores, and v_p is the volume fraction of pores in carbon matrix (Eq. (10)).

$$v_p = \frac{v_3(\text{pore})}{v_2(\text{carbon matrix}) + v_3(\text{pore})} \quad (10)$$

Next, the thermal conductivity of carbon containing Al_2O_3 and pores (κ_{ap}) is given by Eq. (11),

$$\kappa_{ap} = \kappa_m - \kappa_m v_a^{2/3} \left[1 - \frac{1}{1 - v_a^{1/3} \left(1 - \frac{\kappa_m}{\kappa_1} \right)} \right] \quad (11)$$

where κ_1 is the thermal conductivity of Al_2O_3 and v_a is volume fraction of Al_2O_3 in carbon- Al_2O_3 -pore system (Eq. (12)).

$$v_a = \frac{v_1(\text{Al}_2\text{O}_3)}{v_1(\text{Al}_2\text{O}_3) + v_2(\text{carbon matrix}) + v_3(\text{pore})} \quad (12)$$

Finally, the thermal conductivity of carbon- Al_2O_3 -SiC-pore system (κ_b) is given by Eq. (13),

$$\kappa_b = \kappa_{ap} - \kappa_{ap} v_4^{2/3} \left[1 - \frac{1}{1 - v_4^{1/3} \left(1 - \frac{\kappa_{ap}}{\kappa_4} \right)} \right] \quad (13)$$

where κ_4 is the thermal conductivity of SiC and v_4 is volume fraction of SiC in carbon- Al_2O_3 -SiC-pore system (Eq. (14)).

$$v_4 = \frac{v_4(\text{SiC})}{v_1(\text{Al}_2\text{O}_3) + v_2(\text{carbon matrix}) + v_3(\text{pore}) + v_4(\text{SiC})} = \frac{v_4(\text{SiC})}{1} \quad (14)$$

In carbon- Al_2O_3 - SiO_2 -pore system, the parameters κ_4 and v_4 for SiC in Eqs. (13) and (14) are changed to κ_5 and v_5 for SiO_2 in Table 1, respectively, to calculate κ_b .

4.2 Calculated thermal conductivity

Figures 6 and 7 show the calculated conductivities of carbon- Al_2O_3 -SiC-pore system (sample B) and carbon- Al_2O_3 - SiO_2 -pore system (sample C), respectively. In Figs. 6 and 7, SiC and SiO_2 contents were fixed to be 3.6 and 19.1 vol%, respectively. The three points (i, ii and iii) indicated in Fig. 6 show the thermal conductivity for two phase systems (C-SiC,

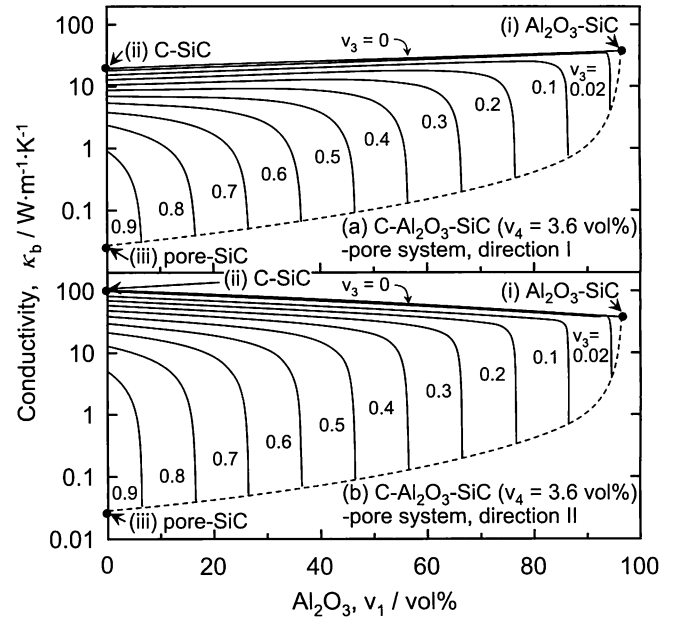


Fig. 6 Calculated conductivity of carbon- Al_2O_3 -SiC-pore system. v_1 : volume fraction of Al_2O_3 , v_3 : volume fraction of pore, v_4 : volume fraction of SiC, κ_b : calculated thermal conductivity of carbon- Al_2O_3 -SiC-pore system.

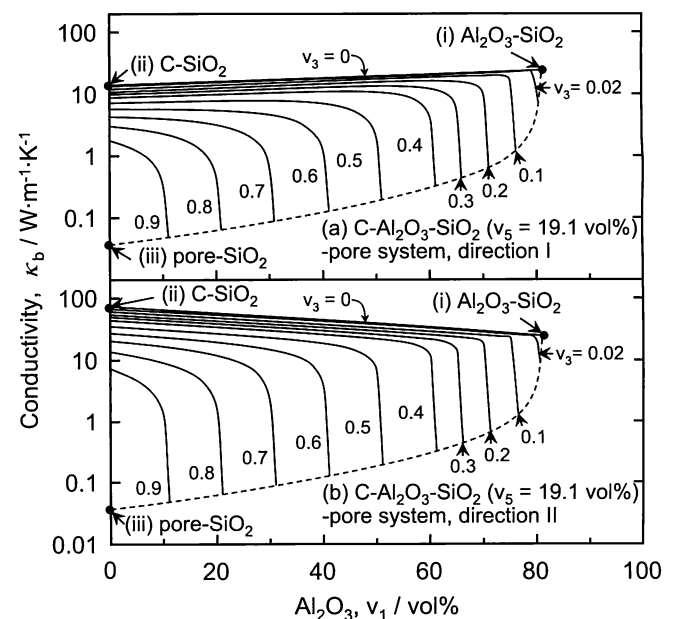


Fig. 7 Calculated conductivity of carbon- Al_2O_3 - SiO_2 -pore system. v_1 : volume fraction of Al_2O_3 , v_3 : volume fraction of pore, v_5 : volume fraction of SiO_2 , κ_b : calculated thermal conductivity of carbon- Al_2O_3 - SiO_2 -pore system.

Al₂O₃-SiC, pore-SiC) with a fixed SiC content ($v_4 = 3.6$ vol%). The line for v_3 (pore) = 0 vol% along the directions I and II of graphite structure in Fig. 6 represent the κ_b for three phase system of C-Al₂O₃-SiC ($v_3 = 0$ vol%, $v_4 = 3.6$ vol%). It is noted that the Al₂O₃-SiC point is plotted at v_1 (Al₂O₃ content) = 96.4 vol% because of a fixed value of $v_4 = 3.6$ vol%. The each conductivity of C-SiC, Al₂O₃-SiC and pore-SiC in directions I and II is higher than that of C, Al₂O₃ and pore in Fig. 4, respectively, because of the addition of SiC grains with a high thermal conductivity. The calculated tendency in Fig. 6 is very similar to that in Fig. 4. That is, it is possible to interpret the results in Fig. 6 with the microstructure-thermal conductivity relation shown in Fig. 5. In four phase systems, carbon, Al₂O₃ and pore are changed to carbon with SiC, Al₂O₃ with SiC and pore with SiC, respectively.

In Fig. 7, κ_b for a fixed SiO₂ content ($v_5 = 19.1$ vol%) is calculated. Since the thermal conductivity of SiO₂ grains is lower than that of carbon matrix or Al₂O₃ grains (Table 1), the κ_b value at point C-SiO₂ in directions I and II is lower than the κ_b value at point of carbon in Fig. 4. A similar relation is also recognized between point Al₂O₃-SiO₂ in Fig. 7 and point Al₂O₃ in Fig. 4. However, the κ_b value at point of pore-SiO₂ is higher than that at point of pore in Fig. 4 because of κ_p (pore) < κ_5 (SiO₂).

5. Comparison between measured and calculated thermal conductivities

Figure 8 summarizes the calculated thermal conductivities of samples A, B and C. The values in parentheses show the compositions (Table 1) of phases present in the refractory brick. The calculated value reflects the integrated effect of (1) only the carbon matrix (graphite plus amorphous carbon), (2) carbon matrix containing pores (two phase systems), (3) carbon matrix containing pores and Al₂O₃ inclusion (three phase systems) and (4) carbon matrix-pores-Al₂O₃ grains-SiC (or SiO₂) grains (four

phase systems) in directions I and II of graphite structure in Fig. 3. The thermal conductivities in directions I and II in Fig. 8 were calculated for the carbon matrix with the orientation of c-axis of graphite in Fig. 3 using the thermal conductivity by Eqs. (5) and (8), respectively. At first, we see the integrated effect of three phase systems in Fig. 8(a). The thermal conductivity of carbon matrix, which is affected by the orientation of graphite structure and the volume fractions of graphite and amorphous carbon, decreases drastically with the introduction of pores in refractory brick. The addition of Al₂O₃ grains increases κ_b in direction I but decreases slightly κ_b in direction II. This difference is discussed in Section 3.3 and depends on the magnitude of κ_{ap} (carbon containing pores) and κ_1 (alumina). When no preferred orientation of graphite structure is produced, an isotropic thermal conductivity may be measured for both the directions I and II in Fig. 3. The difference in the measured thermal conductivities in two directions became smaller in the order of sample B > sample C > sample A. In addition, the difference of κ_b values in two directions were larger for the calculation than for the experiment. This indicates that (1) the calculation provides the maximum and minimum κ_b values and (2) the degree of preferred orientation of graphite structure in refractory brick is smaller than the model structure in Fig. 3. The significant result is the nice agreement of the average thermal conductivity between the measurement (30.3 W·m⁻¹·K⁻¹) and calculation (30.2 W·m⁻¹·K⁻¹). This suggests that (1) the actual thermal conductivity for a statically random structure of graphite is very close to the average value of calculated minimum and maximum conductivities, (2) the Al₂O₃ grains and pores are isotropically included in the refractory brick. Further discussion is to derive the conduction model for a statically random structure of graphite present in the refractory brick, which is not treated in this paper. In the four phase system of sample B, a similar effect of pores or alumina inclusion is observed. Addition of a small amount of SiC (3.6 vol%) with a

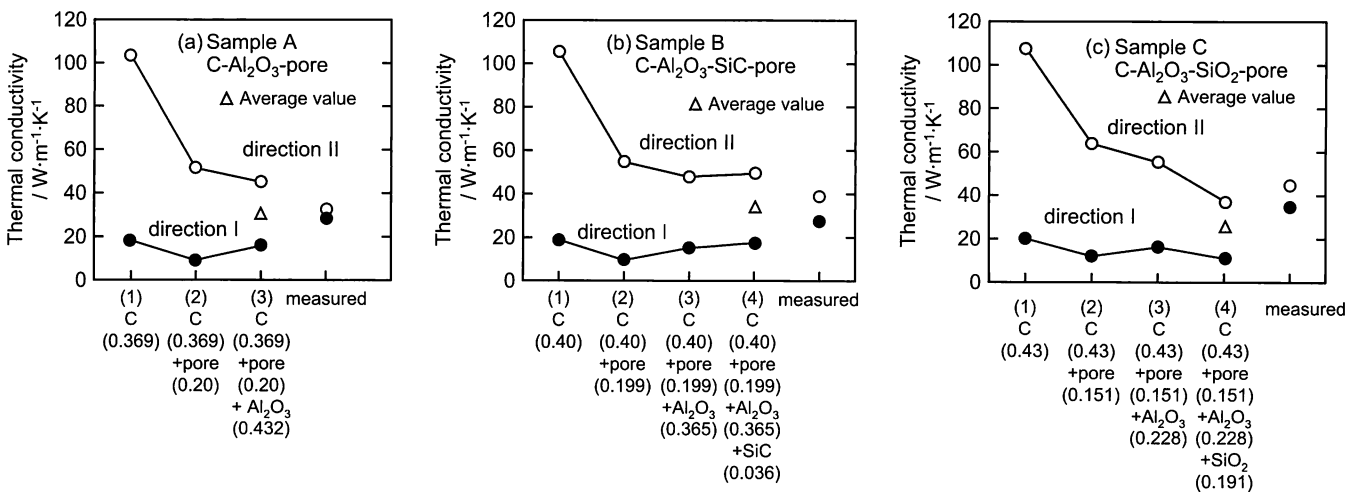


Fig. 8 Comparison between measured and calculated conductivities of (a) carbon-Al₂O₃-pore system, (b) carbon-Al₂O₃-SiC-pore system and (c) carbon-Al₂O₃-SiO₂-pore system. The values in parentheses show the compositions (Table 1) of phases present in the refractory brick. The calculated value reflects the integrated effect of (1) only the carbon matrix (graphite plus amorphous carbon), (2) carbon matrix containing pores (two phase systems), (3) carbon matrix containing pores and Al₂O₃ inclusion (three phase systems) and (4) carbon matrix-pores-Al₂O₃ grains-SiC (or SiO₂) grains (four phase systems) in directions I and II of graphite structure in Fig. 3.

higher conductivity causes a slight increase of κ_b in both the directions. The measured κ_b values were 38.8 and $27.4 \text{ W} \cdot \text{m}^{-1} \cdot \text{K}^{-1}$ (Table 1) and the average value was $33.1 \text{ W} \cdot \text{m}^{-1} \cdot \text{K}^{-1}$. The average value for the calculated two κ_b values (16.3 and $48.6 \text{ W} \cdot \text{m}^{-1} \cdot \text{K}^{-1}$) is $32.5 \text{ W} \cdot \text{m}^{-1} \cdot \text{K}^{-1}$ and close to the measured average thermal conductivity. As seen in Fig. 8(a) and (b), it is apparent that the distribution of pores in the refractory brick, especially in direction II, is the most dominant factor controlling the effective thermal conductivity.

In sample C shown in Fig. 8(c), the addition of Al_2O_3 grains decreases κ_b in direction II because of κ_m (carbon matrix containing pores, Eq. (9)) $> \kappa_1$ (Al_2O_3), and increases κ_b in direction I owing to $\kappa_m < \kappa_1$. Further addition of SiO_2 grains with a lower thermal conductivity reduces both the κ_b values in directions I and II. However, the calculated average κ_b value ($24.3 \text{ W} \cdot \text{m}^{-1} \cdot \text{K}^{-1}$) is relatively lower than the measured κ_b values (34.5 and $44.7 \text{ W} \cdot \text{m}^{-1} \cdot \text{K}^{-1}$, average value $39.6 \text{ W} \cdot \text{m}^{-1} \cdot \text{K}^{-1}$, Table 1). This may be due to the relatively large size of SiO_2 grains shown in Fig. 1(c). The basic equations (2) and (4) in Section 3.1 or equations (9), (11) and (13) in Section 4.1 are derived under the models that all the continuous matrix phase and inclusion (pores and grains) transport the thermal energy to the direction of a lower temperature. When the size of inclusion with a significantly low thermal conductivity such as SiO_2 or air (pores) becomes large, the local region of a high resistance of thermal conduction is formed in refractory brick. In this region, the thermal energy flows along the path of a low resistance of thermal conduction around large pores of SiO_2 grains. That is, pores or SiO_2 grains of large sizes may not contribute to convey the thermal energy. This discussion leads to the approximation of v_s (SiO_2) = 0 vol% in Eq. (13) and the κ_b in sample C is calculated as three phase system of carbon- Al_2O_3 grains-pores. Since the sizes of pores are smaller than those of SiO_2 grains in sample C, the contribution of pores for thermal transportation is included in the calculation. The κ_b values for this three phase system in direction I and II are 16.0 and $54.6 \text{ W} \cdot \text{m}^{-1} \cdot \text{K}^{-1}$ (Fig. 8(c)). The calculated average value for the three phase system is $35.3 \text{ W} \cdot \text{m}^{-1} \cdot \text{K}^{-1}$ and closer to the measured average κ_b value ($39.6 \text{ W} \cdot \text{m}^{-1} \cdot \text{K}^{-1}$). The size effect of inclusion is an important issue and to be treated as a future work in the thermal conductivity of multi phase material.

6. Influence of local structure on thermal conductivity of refractory brick

As seen in Fig. 8, the preferred orientation of graphite structure provides the great influence on the thermal conductivity (calculated values) of refractory brick. However, the degree of actual preferred orientation of graphite structure is smaller than the model structure (Fig. 3) as discussed in Chapter 5. In this Chapter, more complex structure is proposed to calculate the thermal conductivity of a continuous carbon matrix phase.

Figure 9 shows laminated complex structures of amorphous carbon and graphite. The thermal energy is transported from left to right side in these models. The effective thermal conductivity

(κ_c) for the structure of Fig. 9(a) is given by Eq. (15),

$$\kappa_c = \frac{\kappa_{c1}\kappa_{c2}}{\kappa_{c2}\left(\frac{L_{c1}}{L_{c1}+L_{c2}}\right) + \kappa_{c1}\left(\frac{L_{c2}}{L_{c1}+L_{c2}}\right)} \quad (15)$$

where κ_{c1} and κ_{c2} are related to $\kappa_g(\text{II})$ (thermal conductivity of graphite in direction II), $\kappa_g(\text{I})$ (thermal conductivity of graphite in direction I), L_g (thickness of graphite), L_c (thickness of amorphous carbon), S_g (surface area ratio of graphite) and S_c (surface area ratio of amorphous carbon) by Eqs. (16) and (17).

$$\kappa_{c1} = \kappa_g(\text{II})S_g + \kappa_{ac}S_{ac} \quad (16)$$

$$\kappa_{c2} = \frac{\kappa_g(\text{I})\kappa_{ac}}{\kappa_g(\text{I})\left(\frac{L_c}{L_g+L_c}\right) + \kappa_{ac}\left(\frac{L_g}{L_g+L_c}\right)} \quad (17)$$

On the other hand, the effective thermal conductivity for further complex structure shown in Fig. 9(b) is given by Eq. (18),

$$\kappa_b = \kappa_A S_A + \kappa_B S_B \quad (18)$$

where κ_A is equal to κ_{c1} (Eq. (16)) in Fig. 9(a) and κ_B is same as κ_c (Eq. (15)). The S_A and S_B values are surface area ratio ($S_A + S_B = 1$). The microstructure of sample B (Fig. 1(b)) was characterized by the schematic structure in Fig. 9(b) to analyze the thermal conductivity of carbon matrix.

Figure 10 shows the comparison of thermal conductivities between (a) simple structure model (Fig. 3) and (b) complex structure model (Fig. 9(b)) of carbon matrix for sample B. The values in parenthesis show the compositions (Table 1) of phases present in the refractory brick. As compared with simple structure model, the difference of thermal conductivities in two directions I and II becomes smaller for the complex structure model. The calculated average conductivity for four phase system decreases from $32.5 \text{ W} \cdot \text{m}^{-1} \cdot \text{K}^{-1}$ for Fig. 10(a) to $30.7 \text{ W} \cdot \text{m}^{-1} \cdot \text{K}^{-1}$ for Fig. 10(b). However, the measured average thermal conductivity ($33.1 \text{ W} \cdot \text{m}^{-1} \cdot \text{K}^{-1}$) is closer to the

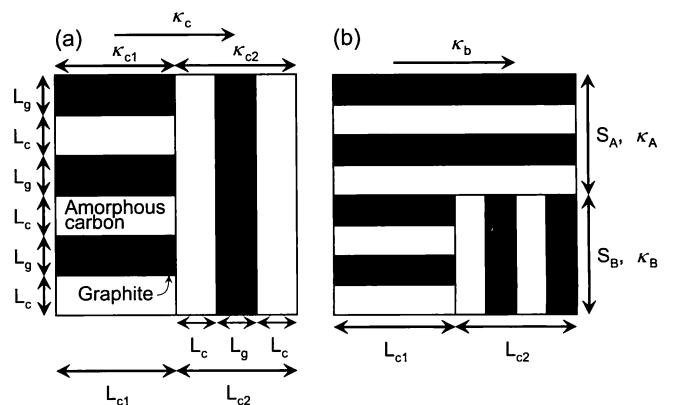


Fig. 9 Complex microstructure models of carbon matrix. κ_c : thermal conductivity of Eq. (15), κ_{c1} : thermal conductivity of Eq. (16), κ_{c2} : thermal conductivity of Eq. (17), κ_b : thermal conductivity of Eq. (18), L_g : thickness of graphite layer, L_c : thickness of amorphous carbon layer, L_{c1} , L_{c2} : length of carbon matrix layer, S : surface area ratio ($S_A + S_B = 1$).

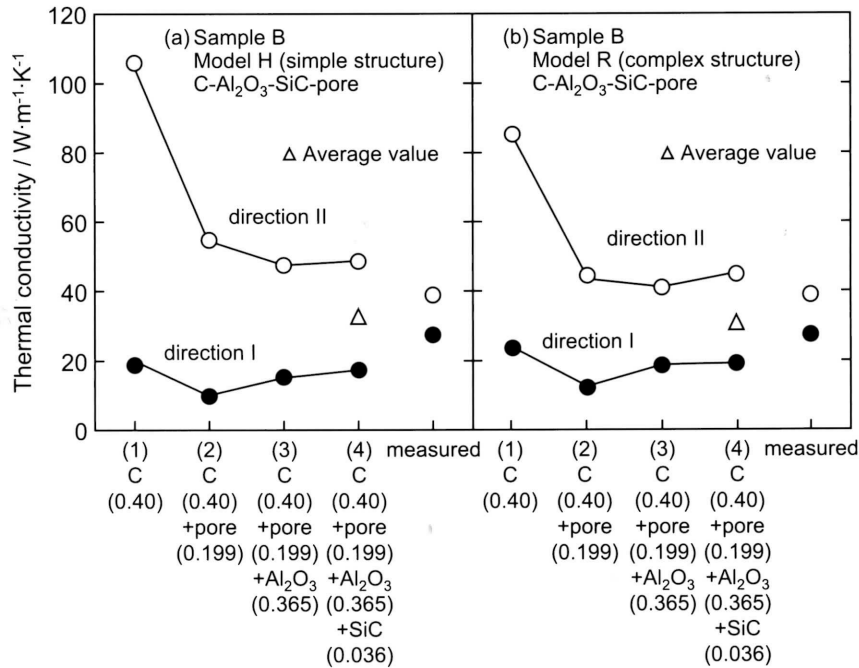


Fig. 10 Comparison between measured and calculated conductivities of carbon-Al₂O₃-SiC-pore system for (a) simple structure model (Fig. 3) and (b) complex structure model of carbon matrix (Fig. 9(b)). The values in parentheses show the compositions (Table 1) of phases present in the refractory brick. The calculated value reflects the integrated effect of (1) only the carbon matrix (graphite plus amorphous carbon), (2) carbon matrix containing pores (two phase systems), (3) carbon matrix containing pores and Al₂O₃ inclusion (three phase systems) and (4) carbon matrix-pores-Al₂O₃ grains-SiC grains (four phase systems) in directions I and II of graphite structure.

calculated average value for Fig. 10(a). Therefore, the careful analysis of local structure of carbon matrix is needed to reflect the microstructure in the thermal conductivity of refractory brick.

7. Conclusions

The thermal conductivity of multi phase refractory brick was calculated based on two phase conduction model developed for solid material with particulate inclusion. The introduction of pores in dense carbon-alumina refractory brick decreases drastically the effective thermal conductivity. The effective thermal conductivity at a given volume fraction of pores, decreases suddenly at a critical volume fraction of Al₂O₃ grains, where carbon matrix disappears. A similar tendency is also observed in four phase systems (carbon matrix-alumina grain-SiC grain (or SiO₂ grain)-pore system). The proposed model provides the maximum and minimum conductivities in parallel and perpendicular directions to c-axis of graphite. A good agreement was recognized between the calculated average conductivity and measured average conductivity. The degree of preferred orientation of graphite structure is smaller for actual

refractory than for the simple structure model used. The complex structure model of a lower preferred orientation of graphite structure, based on the microstructure of refractory brick, provides a smaller difference between maximum and minimum thermal conductivities.

Acknowledgment

This work was financially supported by the Technical Association of Refractories, Japan (2011).

References

- 1) M. Wang and N. Pan, Mater. Sci. Eng., **R63**, 1-30 (2008).
- 2) J. Wang, J. K. Carson, M.F. North and D.J. Cleland, Inter. J. Heat Mass Transfer, **51**, 2389-2397 (2008).
- 3) A. Bouchair, Building and Environment, **43**, 1603-1618 (2008).
- 4) Y. Hirata, Ceram. Inter., **35**, 2921-2926 (2009).
- 5) K. Hata (Ed), Chemical Handbook, Basic Part II (Third Edition), 73-74, The Chemical Society of Japan, Maruzen, Tokyo, (1984).
- 6) Website of Pacific Rundum Co., Ltd., <http://www.rundum.co.jp/product/index6.html>